

Developments on analytic continuation from imaginary chemical potential

Marco Aliberti,* Francesco Di Renzo, Petros Dimopoulos and Demetrianos Gavriel

University of Parma

Parco Area delle Scienze 7/A, Parma, Italy

INFN, Istituto Nazionale di Fisica Nucleare

*E-mail: marco.aliberti@unipr.it, francesco.direnzo@unipr.it,
petros.dimopoulos@unipr.it, demetrianos.gavriel@unipr.it*

Computations at imaginary values of chemical potential are one of the most popular ways to tackle the sign problem in lattice simulations. For this reason, it is important to study more than one way for performing the analytic continuation onto the real axis. In these proceedings we report on different techniques of analytic continuation in this context as a means of getting better control on the systematic effects. In particular, by using lattice data generated by the Bielefeld-Parma collaboration, we compare results which are produced thanks to a novel method that makes use of the Cauchy integral formula with results obtained by other known methods, including the analytic continuation of multi-point Padé approximants.

*The 42nd International Symposium on Lattice Field Theory (LATTICE2025)
2-8 November 2025
Tata Institute of Fundamental Research, Mumbai, India*

*Speaker

1. Motivation

The QCD phase diagram remains, to a large extent, unexplored [1]. A major obstacle in this respect is the presence of the sign problem, which prevents the direct application of lattice QCD techniques at nonvanishing chemical potential. While lattice discretization provides the most reliable framework for non-perturbative calculations through Monte Carlo simulations, its effectiveness crucially relies on the probabilistic interpretation of the path integral measure. When a finite chemical potential is introduced, the Dirac operator acquires a non-trivial phase and the exponential weight entering the partition function ceases to be real and positive, thereby invalidating standard importance-sampling algorithms [2].

A widely adopted strategy to circumvent this difficulty consists in performing simulations at purely imaginary values of the baryon chemical potential. In this regime, the Dirac determinant remains real and Monte Carlo simulations can be carried out without encountering the sign problem [3, 4]. Physical results at real chemical potential must then be obtained by analytic continuation from imaginary to real values in the $\mu_B - T$ plane. This step, however, is intrinsically delicate, since the available numerical data is restricted to a finite number of points and is affected by statistical uncertainties, which can be significantly amplified by the analytic continuation procedure.

The purpose of this work is to discuss recent progress achieved by our collaboration in addressing these issues, via a new numerical method based on the Cauchy integral formula, which will briefly be explained in the following section. For more information and details we refer the readers to the Conference contribution by F. Di Renzo *et al.* [5].

2. The Cauchy integral formula as an inverse problem

It is known from complex analysis, e.g. see [6], that, if a given function $f : \Omega \subseteq \mathbb{C} \rightarrow \mathbb{C}$ is analytic inside a certain region Ω of the complex plane, Cauchy's integral formula is valid $\forall z_0 \in \Omega$:

$$f(z_0) = \frac{1}{2\pi i} \oint_C \frac{f(z)}{z - z_0} dz, \quad (1)$$

where $C = \partial\Omega$ is the oriented contour of region Ω .

The boundary C can be naturally deformed to a circle. In the case that this is centered at the origin of the complex plane with radius R , without crossing any singularity of the function, Eq. (1) can be rewritten as:

$$f(z_0) = \frac{1}{2\pi} \int_{[2\pi]} \frac{Re^{i\theta} f(Re^{i\theta})}{Re^{i\theta} - z_0} d\theta, \quad (2)$$

where we have set $z = Re^{i\theta}$ and the expression $\int_{[2\pi]} \{ \dots \} d\theta$ means that the integration is performed over any interval of amplitude 2π , such as $\theta \in [-\pi, \pi)$ or $\theta \in [0, 2\pi)$.

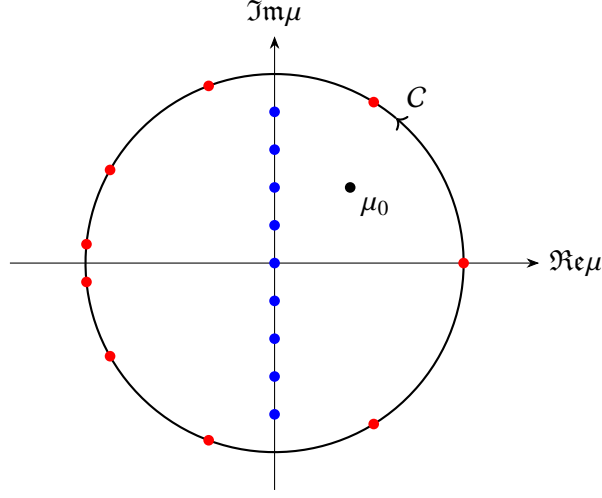


Figure 1: Schematic representation of the Cauchy integral formula, where the analyticity region Ω is taken to be a circle centered at the origin. The blue dots represent known values on the imaginary axis, the red dots represent the Gauss-Legendre quadrature points.

We now consider the case of the n -th cumulant of the net baryon density, which is defined by the following formula:

$$\chi_n(T, V, \mu_B) = \left(\frac{\partial}{\partial \mu_B} \right)^n \frac{\ln \mathcal{Z}(T, V, \mu_B)}{VT^3} \quad (3)$$

where $\mathcal{Z}(T, V, \mu_B)$ is the grand canonical partition function. Here, we focus on the first cumulant, i.e., $n = 1$. Lattice simulations can provide estimates for χ_1 at imaginary values of the chemical potential, $\mu_I = \mu_B$; hence, by applying Eq. (2), we get:

$$\chi_1(\mu_I) = \frac{1}{2\pi} \int_{[2\pi]} \frac{Re^{i\theta} \chi_1(Re^{i\theta})}{Re^{i\theta} - \mu_I} d\theta. \quad (4)$$

The integral above can be approximated by Gauss-Legendre quadrature [7], for which we can write:

$$\chi_1(\mu_I) \simeq \frac{1}{2\pi} \sum_{k=1}^N w_k \frac{Re^{i\theta_k}}{Re^{i\theta_k} - \mu_I} \hat{\chi}_k, \quad (5)$$

where θ_k are the roots of the Legendre polynomials, w_k are their associated weights, and $\hat{\chi}_k$ denote the (unknown) values of $\chi_1(Re^{i\theta})$ evaluated at $\theta = \theta_k$. In principle, N can be any natural number, but for the time being, we will take it to be equal to the total number of conditions we want to impose. A schematic representation of this quadrature is provided in Figure 1.

Furthermore, one could also make use of the Cauchy integral formula applied to function derivatives and the relative approximation given by the Gauss-Legendre quadrature. For the case of the derivatives of χ_1 (following the n -th cumulant definition (3), the m -th derivative of χ_1 will be the $(m + 1)$ -th cumulant and will be denoted as $\chi_{1,m}$) we write:

$$\chi_{1,m}(\mu_I) = \frac{m!}{2\pi i} \oint_C \frac{\chi_{1,m}(\mu)}{(\mu - \mu_I)^{m+1}} d\mu \simeq \frac{m!}{2\pi} \sum_{k=1}^N w_k \frac{Re^{i\theta_k}}{(Re^{i\theta_k} - \mu_I)^{m+1}} \hat{\chi}_k. \quad (6)$$

3. System of equations and Tikhonov regularization

As seen in the previous section, we need to solve a system of N equations in N unknowns, represented by the possible $\hat{\chi}_k$, $k = 1, \dots, N$. Each of the equations can be either in the form of Eq. (5) or in the form of Eq. (6).

In other words, we can represent the system of equations as a matrix equation $AX = B$, where:

$$A_{jk} = \frac{1}{2\pi} w_k \frac{Re^{i\theta_k}}{(Re^{i\theta_k} - \mu_j)^{m+1}}, \quad X_k = \hat{\chi}_k, \quad B_j = \chi_{1,m}(\mu_j), \quad (7)$$

$$j, k = 1, \dots, N, \quad m = 0, 1, 2, \dots$$

However, this system of equations is ill-posed, mainly for two reasons: the first is that the values $\chi_1(\mu_I)$ obtained by lattice simulations are affected by statistical errors; the second is that Eqs (5) and (6) are approximations of the “true” equations valid in the complex plane, which would require an infinite number of points to be applied. Therefore, they represent numerical approximations rather than exact equalities.

For these reasons, it is not advisable to solve this linear system with usual methods, such as finding the vector X for which the square norm $\|AX - B\|^2$ is minimized, unless one wants to deal with high instabilities in the output under slight changes in the input. One possible workaround to this problem is provided by the Tikhonov regularization [8]: a regulator α , called Tikhonov parameter, is introduced, and instead of minimizing $\|AX - B\|^2$, we minimize the expression $\|AX - B\|^2 + \|\alpha X\|^2$ for given α (more details on how to choose this parameter are given below).

Once the values $\hat{\chi}_k$ have been evaluated for $k = 1, \dots, N$, they can be used to perform the analytic continuation either by directly applying Eq. (5) to points on the real axis, or by applying Eq. (6) to a particular point (usually the origin), computing a certain number of derivatives, and using them to build an expansion (Taylor or Padé) that is then evaluated on the real axis.

4. Analytic continuation

As previously stated, there are two main methods to perform the analytic continuation: the direct evaluation on the real axis and the computation of a certain number of derivatives in order to build a truncated expansion. The former method has been explained in [9, 10]; in this work, we will focus on the latter.

Let us suppose that we know the values of the baryon number density $\chi_1(\mu_I)$ on a certain number of points on the imaginary axis (each one with its own statistical uncertainty). From these points, let us select a subset and write equations of the type of Eq. (5). Moreover, we might use the fact that out of the even derivatives of χ_1 , N_D of them are zero at $\mu_I = 0$; so, we can write down an extra set of N_D equations of the form of Eq. (6):

$$\frac{(2m)!}{2\pi} \sum_{k=1}^N w_k \frac{\hat{\chi}_k}{(Re^{i\theta_k})^{2m}} = 0, \quad m = 1, \dots, N_D. \quad (8)$$

By doing this, we are effectively imposing the charge conjugation symmetry to hold up to a certain order¹. Furthermore, if desired, one could also impose the *Cauchy condition*:

$$0 = \oint_C \chi_1(\mu) d\mu \simeq \sum_{k=1}^N R e^{i\theta_k} w_k \hat{\chi}_k, \quad (9)$$

that is equivalent to imposing that $\chi_1(\mu)$ is analytic inside the region bounded by C .

The total number N of unknowns $\hat{\chi}_k$ is chosen to be equal to the total number of equations. We can then solve the linear system to evaluate a certain number of derivatives at a particular point, the origin, and build a truncated Taylor expansion around that point, which we can use to approximate the *true* baryon number density. In addition, we could also build a single-point Padé approximant in order to have two different approximations of $\chi_1(\mu)$.

4.1 Single-point Padé approximant

The single-point Padé approximant of a function $f(\mu)$ around $\mu = \mu_0$ is a rational function obtained as the ratio of two polynomials, $P_m(\mu)$ and $Q_n(\mu)$, of degree m and n , respectively:

$$R_n^m(\mu) \equiv \frac{P_m(\mu)}{Q_n(\mu)} = \frac{\sum_{k=0}^m p_k (\mu - \mu_0)^k}{1 + \sum_{j=1}^n q_j (\mu - \mu_0)^j}. \quad (10)$$

The $m+n+1$ coefficients $p_0, \dots, p_m, q_1, \dots, q_n$ are fixed such that the first $m+n+1$ derivatives of $R_n^m(\mu)$ evaluated at $\mu = \mu_0$ are equal to the first $m+n+1$ derivatives of the function $f(\mu)$ evaluated at the same point μ_0 .

The advantage of performing a Padé approximant over a Taylor series expansion is that the former can also interpolate the singularities of the underlying function as poles. The Padé approximant can also *codify* other types of singularities; for example, branch-cuts are represented as an interlacing series of zeros and poles originating from the two singularities (not necessarily poles) that delimit the cut [11]. This is relevant in order to look for the critical endpoint of the QCD phase diagram.

4.2 Selecting the optimal Tikhonov parameter

The Tikhonov parameter is tuned as follows. For each value of α in the range 10^{-8} to 10^{-2} (sampling $\sim 10^5$ – 10^6 values), the system of equations is solved to determine the coefficients $\hat{\chi}_k$. For each of these values of α , a Taylor expansion and a Padé approximant are constructed. The corresponding χ^2 is then computed with respect to the input data that has not been used in setting up the equations.

The optimal Tikhonov parameter is then chosen to be the one corresponding to the least value of the χ^2 , separately for the Taylor expansion and the Padé approximant.

¹The charge conjugation symmetry would require the function $\chi_1(\mu)$ to be odd, thus all its even derivatives should be 0 when evaluated at the origin, i. e., $\chi_{1,2m}(0) = 0 \forall m \in \mathbb{N}$.

5. Systematics

5.1 Near-contour imprecisions and angle dependence

The first source of systematic errors is due to numerical approximations that become important when the evaluated points are near the contour of integration, likely due to the denominator approaching zero. Furthermore, these imprecisions change their location on the complex plane based on the chosen 2π interval of integration for the variable θ . This has been tested on known analytic functions, of which, the function $f(z) = \sin(z)$ is reported in Figure 2.

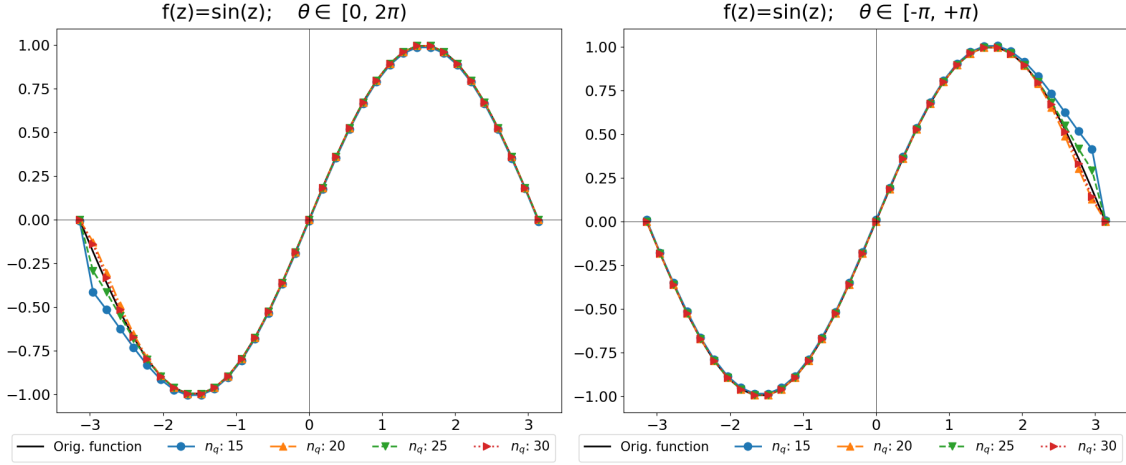


Figure 2: Near-contour imprecisions and θ parameter dependence obtained by directly applying the Cauchy formula on the function $\sin(z)$. Different colors represent different numbers of integration points. For all the plots, a radius of $R = \pi + 0.001$ has been used to perform the integration.

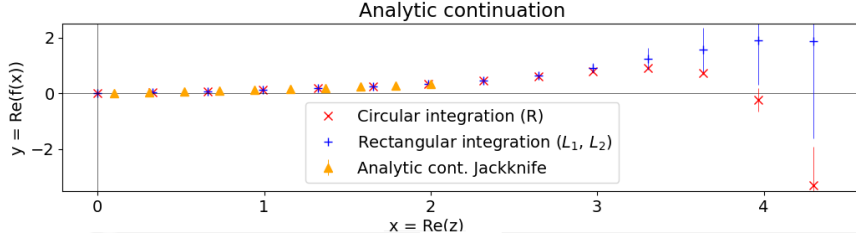
As it can be seen, there are some *artifacts* that appear for negative values of the real axis, for the real part of the function (Figure 2, left), when the interval $\theta \in [0, 2\pi)$ is used, while for positive values of the real axis these artifacts are not observed. This situation is flipped if the interval chosen is $\theta \in [-\pi, \pi)$, as in Figure 2, right.

These artifacts have been observed for different analytic functions and for other choices of the θ interval, although they are not reported here for brevity.

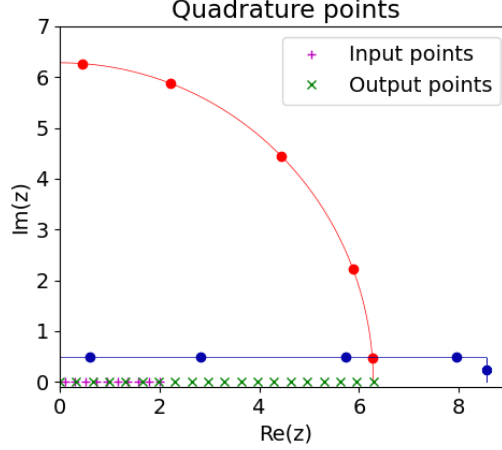
5.2 Different contours and contour-parameter dependence

Regarding formula (1), choosing the integration contour C to be a circumference is not mandatory. In fact, one is free to choose C as long as the function $f(z)$ is analytic $\forall z \in \Omega$, the region bounded by C . In other words, the integration contour C can be continuously deformed into a different one, C' , provided that the deformation never crosses any of the function's singularities.

For this reason, a different type of contour has also been tried: a rectangle of width $2L_1$ and height $2L_2$, centered at the origin and with its sides parallel to the real and imaginary axes, as can be seen in Figure 3b. The input points have been computed by performing a preliminary analytic continuation of the data presented in the following section via a Taylor expansion, and then using the output points of the first analytic continuation to extend further along the real axis.



(a) Analytic continuation of $\chi_1(\mu)$ on the real axis. Error bars are obtained via a jackknife analysis.



(b) Integration contours on the quadrant $\Re\mu \geq 0$, $\Im\mu \geq 0$. The dots represent the quadrature points for the two integration contours.

Figure 3: Analytic continuation performed using two different contours: a circle (red) and a rectangle (blue). The function’s symmetries ($\chi_1(-\mu) = -\chi_1(\mu)$ and $\chi_1(\mu^*) = \chi_1(\mu)^*$) have been used to perform the computation on only one quadrant of the complex μ plane.

The results of the different integrations for the two contours are reported in Figure 3a; there is no clear evidence that choosing the rectangle over the circle leads to better accuracy, as the analytically continued values are compatible with one another after propagating the errors from the input points using a jackknife analysis.

6. Lattice data and numerical results

The previously described procedure, in Section 4, has been applied to the data obtained from the Bielefeld-Parma collaboration through simulations with Highly Improved Staggered Quarks (HISQ), $2 + 1$ flavors, at $T = 157.5$ MeV and $N_\tau = 6$, with physical pion masses. These data are plotted in Figure 4 as black dots (notice the very small error bars).

Three different expansions have been produced: a Taylor expansion up to order μ^9 and two different Padé expansions $R_4^5(\mu)$; the “Padé odd” is a Padé expansion built to be an odd function of the μ variable². As it is clear from the plot, Padé odd is completely superimposed on the standard Padé; therefore, manually imposing the function symmetry $R_4^5(-\mu) = -R_4^5(\mu)$ is superfluous. Note that the symbols for imaginary and real parts in Figures 3 a,d 4 & 5 do not look the same.

²It is built such that the numerator $P_5(\mu)$ consists only of odd powers of μ and the denominator $Q_4(\mu)$ consists only of even powers of μ .

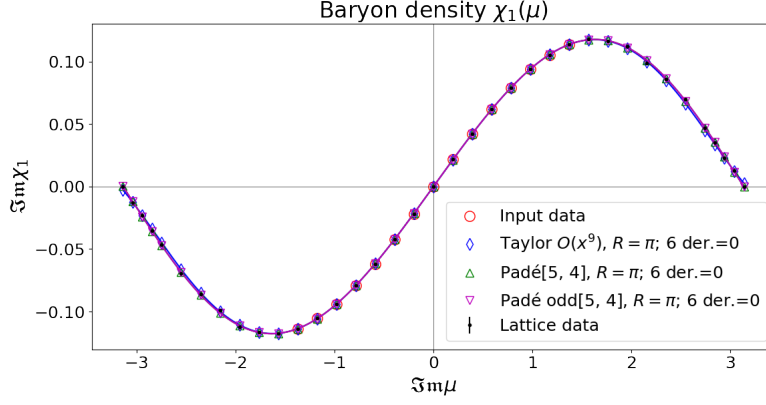


Figure 4: Implementation of the different procedures for analytic continuation. Lattice data for $\text{Im}\chi_1$ computed at imaginary values of the chemical potential, $\text{Im}\mu$ are shown with black dots. Of these data shown as circled in red are the ones used as input in the procedure.

The resulting mean values for the analytic continuation on the real axis, obtained with each method, are plotted in Figure 5, along with a preliminary error analysis for the Taylor method.

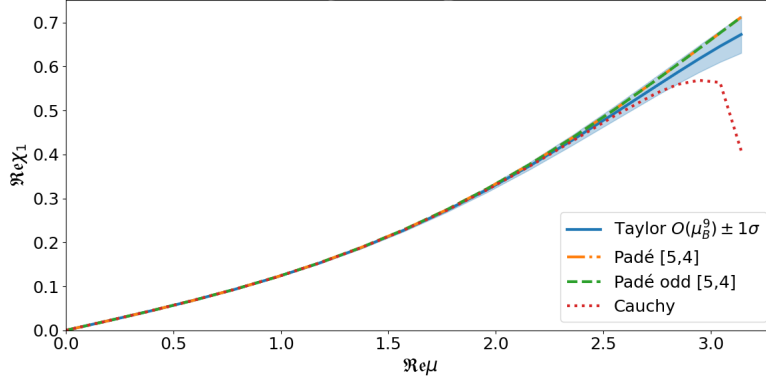


Figure 5: Estimates are shown for the mean values of the net baryon density from analytic continuation onto real values for the chemical potential. Both Taylor and Padé expansions are presented. The error estimate concerning the Taylor expansion has been obtained via a statistical bootstrap. For comparison, the result from the direct application of the Cauchy formula is also shown. Notice that the value $R = \pi$ for the contour radius has been used in this analysis.

The statistical bootstrap has been performed by extracting 1000 random samples from the input data distribution and then selecting only the samples that lead to Taylor expansions that fit the whole set of data with reasonable values of χ^2 . This is still a preliminary analysis; a full error budget analysis will be thoroughly addressed in a forthcoming publication.

6.1 Comparison of our results to the existing literature

With the use of Taylor and Padé expansions, we are also able to obtain estimates for $\chi_1(\mu)$ and its derivatives evaluated at $\mu = 0$. In Table 1, we present the comparison of our estimates with values reported by the HotQCD collaboration [12].

| | Taylor | Padé | HotQCD [12] | |
|----------------|---------------------------|------------------------|--------------------------------------|-------------------------------------|
| | $R = \pi,$ | $N_\tau = 6$ | $\chi_{2,4} \rightarrow N_\tau = 6,$ | $\chi_{6,8} \rightarrow N_\tau = 8$ |
| $\chi_2(0)$ | $1.096(4) \times 10^{-1}$ | 1.098×10^{-1} | $1.087(4) \times 10^{-1}$ | $T = 157.17 \text{ MeV}$ |
| $\chi_4(0)$ | $8.62(17) \times 10^{-2}$ | 8.74×10^{-2} | $8.4(4) \times 10^{-2}$ | |
| $\chi_6(0)$ | $1.8(3.7) \times 10^{-3}$ | 7.3×10^{-3} | $-4(3) \times 10^{-2}$ | $T = 156.91 \text{ MeV}$ |
| $\chi_8(0)$ | $-1.9(8) \times 10^{-1}$ | -2.0×10^{-1} | $-7(9) \times 10^{-1*}$ | |
| $\chi_{10}(0)$ | $-1.5(5) \times 10^{-1}$ | -1.3×10^{-1} | | |

Table 1: Estimates for the first five odd derivatives of $\chi_1(\mu)$, evaluated at $\mu = 0$, owing to Taylor and Padé expansions. The value $R = \pi$ has been imposed for the radius contour in the Cauchy formula. Results from the Taylor expansion are accompanied by the corresponding statistical errors in parentheses; also see [5] for preliminary estimates of systematic uncertainties. In the last column, results from HotQCD collaboration are reported [12], from simulations at similar values of temperature (T) and temporal lattice size (N_τ).

Our results from both Taylor and Padé expansions are nicely compared to the HotQCD ones; as for the Taylor case, for which a preliminary error analysis has been performed, we notice that the results agree within 1-2 σ . Furthermore, our value for $\chi_{10}(0)$ is among the first two estimates appearing in the bibliography for this quantity; see the new preprint [13], where the value $\chi_{10}(0) = -0.016 \pm 0.288$ from lattice simulations at $T = 158.5 \text{ MeV}$ and $N_\tau = 8$ is reported.

Finally, we mention two interesting self-consistency checks. First, we report that our estimate for $\chi_2(0)$ in Table 1 is well compared with a direct lattice computation giving $\chi_2(0) = 1.110 \times 10^{-1} \pm 1.6 \times 10^{-3}$. We should add here that we opted not to use the above value as an input in our analysis due to its higher uncertainty when compared to the χ_1 lattice data. The second check consists of the following observation: values at the quadrature points come in complex conjugate pairs, as should be expected, although this condition has never been explicitly imposed; this is true for both the Taylor and the Padé expansions.

7. Conclusion and outlook

In conclusion, the method we developed provides results for the analytic continuation and the Taylor coefficients of the baryon number density that show remarkable stability with respect to the different methods (Taylor or Padé) and the integration parameters, namely the radius R and the angular variable θ : slight changes in the radius and the choice of the integration interval for the angle θ did not result in sensitive changes in the computed derivatives.

Based on a preliminary analysis, we can provide fairly accurate estimates for higher order derivatives of χ_1 that are in good agreement with the bibliography.

We would like to stress that, thanks to the analytic continuation method we have proposed, the computational cost of obtaining accurate results is far less than the cost required for a direct lattice evaluation of the same quantities. A full study of statistical and systematic uncertainties is underway, and it will be presented in a forthcoming publication.

*Obtained with a different regularization scheme.

Acknowledgments

This work is supported by INFN under the research project *i.s. QCDLAT*. It is our pleasure to thank all our colleagues in the Bielefeld-Parma Collaboration: we plan to apply all this machinery in the context of our common research plans.

References

- [1] S. Borsanyi and P. Parotto, *The QCD phase diagram*, [2512.08843](#).
- [2] G. Aarts, *Introductory lectures on lattice qcd at nonzero baryon number*, *Journal of Physics: Conference Series* **706** (2016) 022004.
- [3] P. de Forcrand and O. Philipsen, *The QCD phase diagram for small densities from imaginary chemical potential*, *Nucl. Phys. B* **642** (2002) 290 [[hep-lat/0205016](#)].
- [4] M. D'Elia and M.-P. Lombardo, *Finite density QCD via imaginary chemical potential*, *Phys. Rev. D* **67** (2003) 014505 [[hep-lat/0209146](#)].
- [5] F. Di Renzo, M. Aliberti, D. Gavriel and P. Dimopoulos, *Finite density lattice QCD as an inverse problem (aka analytical continuation from imaginary to real chemical potential via Cauchy integral formula)*, *PoS LATTICE2025* (2026) 111.
- [6] L.V. Ahlfors, *Complex Analysis*, McGraw–Hill, 3rd ed. (1979).
- [7] W.H. Press, S.A. Teukolsky, W.T. Vetterling and B.P. Flannery, *Numerical Recipes: The Art of Scientific Computing*, Cambridge University Press, 3rd ed. (2007).
- [8] A. Buccini, M. Donatelli and L. Reichel, *Iterated tikhonov regularization with a general penalty term*, *Numerical Linear Algebra with Applications* **24** (2017) e2089.
- [9] M. Aliberti and F. Di Renzo, *Taylor series coefficients at $\mu = 0$ from imaginary μ computations*, *PoS LATTICE2024* (2025) 170.
- [10] F. Di Renzo, M. Aliberti and P. Dimopoulos, *On analytic continuation from imaginary to real chemical potential in Lattice QCD*, *PoS LATTICE2024* (2025) 174 [[2502.03392](#)].
- [11] H. Stahl, *The convergence of padé approximants to functions with branch points*, *Journal of Approximation Theory* **91** (1997) 139.
- [12] HotQCD Collab., D. Bollweg et al., *Taylor expansions and Padé approximants for cumulants of conserved charge fluctuations at nonvanishing chemical potentials*, *Phys. Rev. D* **105** (2022) 074511 [[2202.09184](#)].
- [13] A. Adam, S. Borsányi, Z. Fodor, J.N. Guenther, P. Kumar, P. Parotto et al., *High-precision baryon number cumulants from lattice qcd in a finite box: cumulant ratios, lee-yang zeros and critical endpoint predictions*, [2507.13254](#).